Kinetics and Thermodynamics of the Unfolding and Refolding of the Three-Stranded α-Helical Coiled Coil, Lpp-56[†]

Anatoly I. Dragan,[‡] Sergey A. Potekhin,[§] Andrei Sivolob,[||] Min Lu,[⊥] and Peter L. Privalov*[,‡]

Department of Biology, Johns Hopkins University, Baltimore, Maryland 21218, Institute of Protein Research, Pushchino, Moscow Region, 142290 Russia, Department of General and Molecular Genetics, National University, 01033 Kiev, Ukraine, and Department of Biochemistry, Weill Medical College of Cornell University, New York, New York 10021

Received July 30, 2004; Revised Manuscript Received August 20, 2004

ABSTRACT: Temperature-induced reversible unfolding and refolding of the three-stranded α-helical coiled coil, Lpp-56, were studied by kinetic and thermodynamic methods, using CD spectroscopy, dynamic light scattering, and scanning calorimetry. It was found that both unfolding and refolding reactions of this protein in neutral solution in the presence of 100 mM NaCl are characterized by unusually slow kinetics, which permits detailed investigation of the mechanism of these reactions. Kinetic analyses show that the unfolding of this coiled coil represents a single-stage first-order reaction, while the refolding represents a single-stage third-order reaction. The activation enthalpy and entropy for unfolding do not depend noticeably on temperature and are both significantly greater than those for the folding reaction, which show a significant dependence on temperature. The activation heat capacity change for the unfolding reaction is close to zero, while it is quite significant for the folding reaction. The correlation between the activation and structural parameters obtained for the Lpp-56 coiled coil suggests that interhelical van der Waals interactions are disrupted in the transition state, which is nevertheless still compact, and water has not yet penetrated into the interface; the transition from the transient state to the unfolded state results in hydration of exposed apolar groups of the interface and the disruption of helices. The low propensity for the Lpp-56 strands to fold and associate is caused by the high number of charged groups at neutral pH. On one hand, these charges give rise to considerable repulsive forces destabilizing the helical conformation of the strands. On the other hand, they align the folded helices in parallel and in register so that the apolar sides face each other, and the oppositely charged groups may form salt links, which are important for the formation of the trimeric coiled coil. A decrease in pH, which eliminates the salt links, dramatically decreases the stability of Lpp-56; its structure becomes less rigid and unfolds much faster.

The α-helix and α-helical coiled coils represent fundamental structural motifs in proteins. The relative simplicity of coiled coils suggests that they might be effective models for understanding protein design and the mechanism of folding (*1*−*4*). The folding and unfolding of the single-stranded α-helix and two-stranded α-helical coiled coils have therefore been intensively studied experimentally and theoretically (see refs *5*−*15*). Three-stranded coiled coils have been studied much less (*16*−*19*), although they present considerable interest themselves as biological molecules and also as the next level in modeling globular proteins by a bundle of helices (see refs *20* and *21*).

Here we present the results of studying the unfolding and refolding of the three-stranded α-helical coiled coil, Lpp-56,[1] which is a fragment of a lipoprotein from the outer membrane of *Escherichia coli* (*22*). Crystallographic study of this protein (*23*, *24*) showed that its three helical strands form an apolar core inside the coiled coil and the polar external surface (Figure 1A,B). However, at neutral pH, the three helical strands are held together not only by the hydrophobic forces maintaining the apolar core but also by the salt links between the negatively and positively charged Asp and Lys residues, which become spatially close in the trimeric structure (Figure 1C). Our investigation has revealed a rather unexpected feature of the temperature-induced unfolding and refolding of this protein: both these reactions are extremely slow at neutral pHs. Correspondingly, the experimentally observed melting profiles of this molecule do not reflect a real equilibrium. This causes certain difficulties in studying the energetic bases of the structure of this protein, but it opens prospects for detailed investigation of the dynamics of its formation. Similar situations, when

[†] This work was supported by NIH Grant GM48036-12.

* To whom correspondence should be addressed. Phone: (410) 516-6532. Fax: (410) 261-1064. E-mail: privalov@jhu.edu.

[‡] Johns Hopkins University.

[§] Institute of Protein Research.

[||] National University.

[⊥] Weill Medical College of Cornell University.

[1] Abbreviations: Lpp-56, 56-amino acid polypeptide of the trimeric coiled-coil domain of the *E. coli* outer membrane lipoprotein; C_p, partial molar heat capacity; $C_p^{exc}(T)$, excess heat capacity as a function of temperature; C_p^{max}, heat capacity value at the heat absorption peak; ΔC_p, heat capacity increment upon unfolding of the protein; ΔH^{cal} and ΔH^{vH}, enthalpies measured calorimetrically and determined using the van't Hoff equation, respectively; T_{max} or T_m, temperature of heat absorption maximum at the melting of the coiled coil; T_G, temperature at which the Gibbs energy of the equilibrium unfolding of the protein is zero; T_t, equilibrium transition temperature at which half of the molecules are in the unfolded state in the equilibrium process.

10.1021/bi048365+ CCC: $27.50
Published on Web 11/05/2004

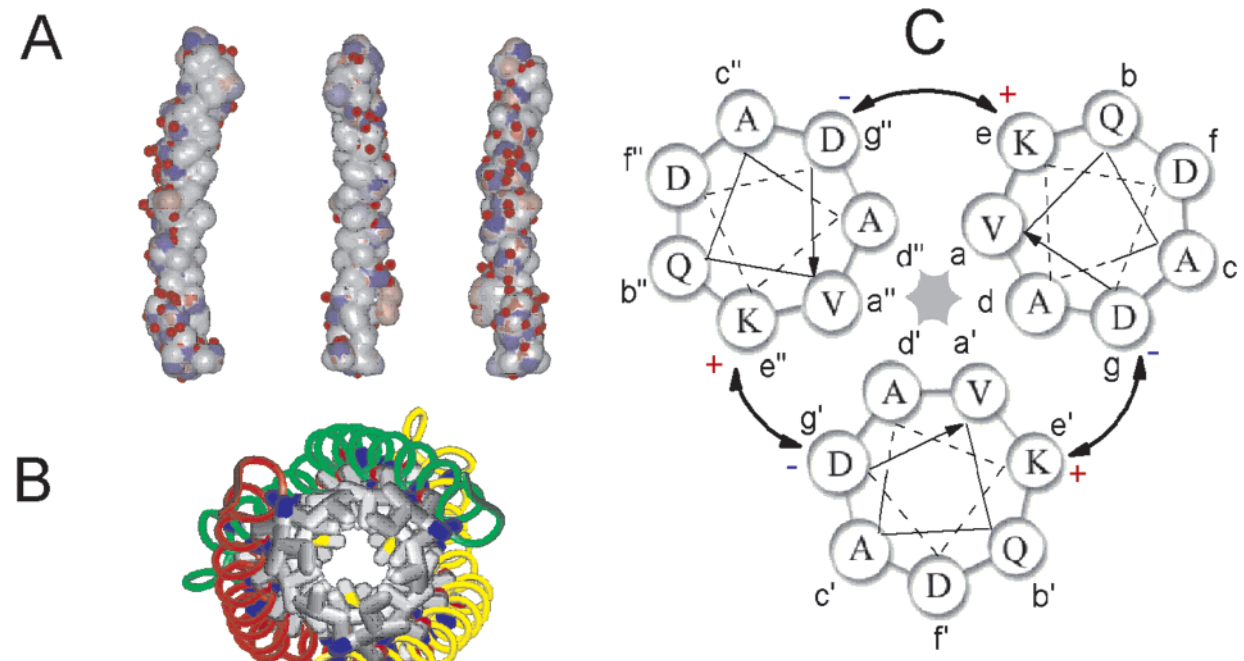

FIGURE 1: (A) Side view of the separated α-helical strands of the Lpp-56 trimeric coiled coil showing that their contact surfaces are apolar and completely dehydrated in contrast to the polar external surfaces, which bind a considerable number of water molecules (immobilized water molecules are shown by the red beads, negative charges are blue, and the red spheres show positively charged Lys and Arg residues). (B) Axial view of Lpp-56 showing the hydrophobic core, which goes along the trimeric coiled coil. (C) Axial slice of Lpp-56 showing formation of the salt links between the Asp and Lys residues at neutral pH. At the bottom is given the sequence of the Lpp-56 polypeptide chain.

the experimentally observed unfolding of protein proceeds far from equilibrium, are rather frequent in protein science and, if not recognized, might raise doubts about the applicability of thermodynamics to proteins in general (see refs *25* and *26*).

MATERIALS AND METHODS

Protein Isolation and Characterization. The Lpp-56 protein was isolated as described in ref *24*. The sequence of the protein is given in Figure 1. Results of MALDI mass spectrometry analysis showed that the protein samples were highly homogeneous, and the estimated molecular mass (6156.3 Da) corresponds well with that calculated from its sequence (6153.7 Da). Concentrations of the Lpp-56 protein in solution were determined spectrophotometrically using an extinction coefficient E_{270} of 1280 M^{-1} cm^{-1}. Experiments were carried out in two standard solutions: 100 mM NaCl, 10 mM sodium phosphate buffer (pH 7.4) and 100 mM NaCl, 10 mM glycine-HCl buffer (pH 3.0). The protein solutions prepared for the experiments, particularly calorimetric, were carefully dialyzed against solvent.

Calorimetry. Calorimetric measurements were carried out on a Nano-DSC instrument (Calorimetric Science Corp.) with capillary calorimetric cells. The advantage of this instrument is that it has a short relaxation time (<20 s), can scan up and down between 0 and 130 °C with a chosen constant rate, and has an exceptionally stable baseline, which is needed for determining the absolute partial heat capacity of a protein over the whole operational temperature range. In the calorimetric experiments with Lpp-56, we used scanning rates from 0.125 to 2.0 K/min, but most of the experiments were carried out at 1.0 K/min. The Nano-DSC instrument is equipped with the software program to run itself and process the measured data, to determine the partial heat capacity as a function of temperature and analyze it (*27*, *28*).

Ellipticity. The ellipticity of the Lpp-56 protein was studied using a JASCO J-710 spectropolarimeter. The temperature was scanned up and down with different fixed rates using a Peltier PTC-3481 temperature controller. In the kinetic experiments, the native protein solution was heated rapidly or the preheated solution was cooled rapidly to the required temperature. For this purpose, we did not need to use stopped-flow equipment because both the unfolding and refolding reactions of Lpp-56 are very slow, proceeding over many minutes. For analysis of the reaction rate, we used the initial part of the recorded kinetics curve in which the contribution of the backward reaction is insignificant.

Light Scattering. Dynamic light scattering experiments were carried out using a DynaPro Molecular Sizing Instrument equipped with a Peltier thermostated cell holder and operated under the control of Dynamics 4.0 data acquisition and analysis software. This instrument measures the intensity of scattered light and estimates the apparent hydrodynamic radius of the averaged scattering macromolecules. A special 12 μL quartz microcuvette was used. All solutions were filtered using a MicroFilter system equipped with 0.1 and 0.02 μm Anodisc filters. In kinetic experiments of refolding, the light scattering was recorded at 50 °C after fast cooling

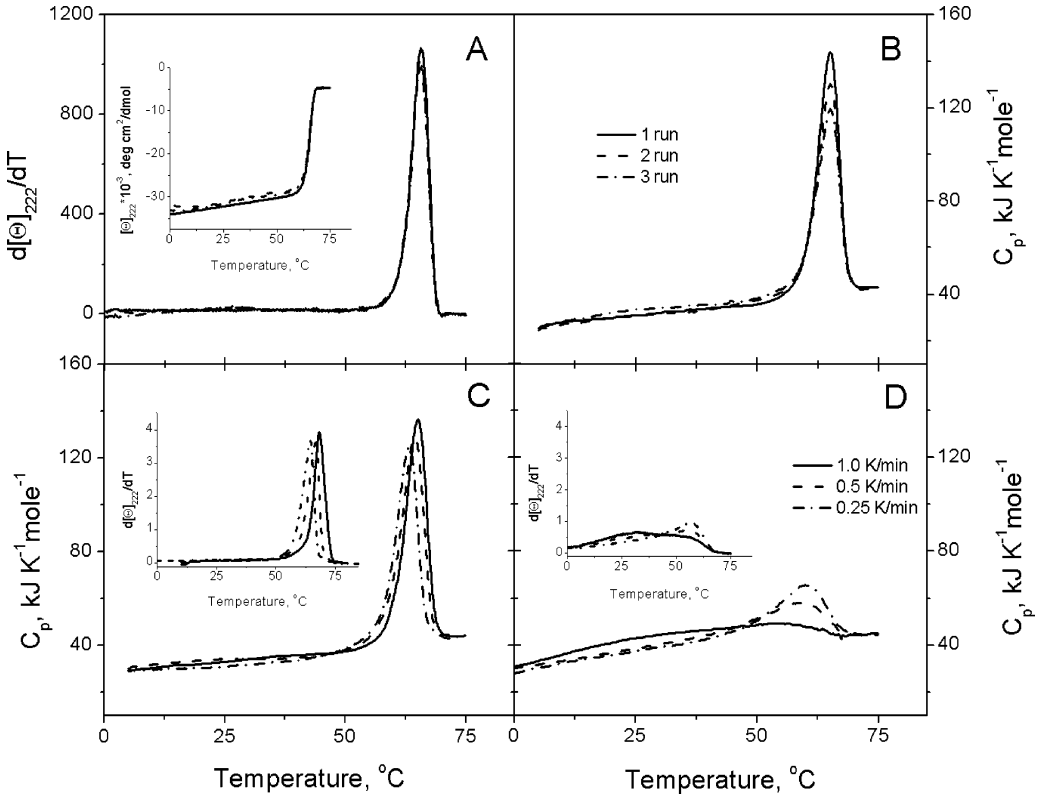

FIGURE 2: (A) Temperature dependencies of the mean residue ellipticity at 220 nm of Lpp-56 at pH 7.4 upon consecutive heatings of the same sample after its slow cooling to the starting temperature of 0 °C (inset), and the temperature derivatives of these functions. (B) Temperature dependencies of the partial molar heat capacity of Lpp-56 upon consecutive heatings of the same sample. (C) Heat capacity functions of Lpp-56 obtained at different heating rates. (D) Heat capacity functions of Lpp-56 obtained at different cooling rates. The concentration of the monomers in all experiments was 210 μM.

from 72 °C. The rate constant was determined by fitting to the experimental curve the function characterizing the third-order reaction:

$$I = I_{unf} + (I_{fld} - I_{unf})[1 - (1 + 18k_{fld}[F_3]^2 t)^{0.5}] \quad (1)$$

where I_{fld} and I_{unf} are the intensities of the scattered light specific for the folded and unfolded protein, respectively, and $[F_3]$ is the concentration of the trimer. In the determination of the radius of gyration, the axial ratio of Lpp-56 was assumed to be 1/5.

Analysis of the Apparent Excess Heat Capacity Profiles. Slow unfolding−refolding kinetics of the Lpp-56 coiled-coil trimer induce deformation of the DSC profiles. Analysis of obtained profiles monitored at different heating and cooling rates can provide information about the rates of unfolding−refolding processes and evaluate thermodynamic parameters in equilibrium.

The excess heat capacity function for the nonequilibrium process is calculated from the equation

$$C_p^{exc}(T) = \Delta H_m \frac{\partial\theta}{\partial T} = \frac{k_{unf}}{V}\left[1 - \theta - (1 - \theta_{eq})\left(\frac{\theta}{\theta_{eq}}\right)^3\right] = \frac{27[F_3]_0^2 k_{fld}}{V}\left(\frac{1 - \theta}{1 - \theta_{eq}}\theta_{eq}^3 - \theta^3\right) \quad (2)$$

where k_{unf} is the rate constant for first-order kinetics of denaturation, k_{fld} is the rate constant for the third-order kinetics of refolding, and V is the heating or cooling rate. $\theta_{eq}(T)$ and $\theta(T)$ are the fractional populations of the denatured form in equilibrium and under experimental nonequilibrium conditions, respectively; $[F_3]_0$ is the concentration of the Lpp-56 trimer. Equation 2 is derived in the Supporting Information. On the basis of this equation, the experimental profiles of Lpp-56 unfolding and refolding were fitted by the lab-made "3M-kinetics" program (which can be requested) and the activation energies (ΔH^*_{unf} and ΔH^*_{fld}), the rate constants of unfolding and refolding (k_{unf} and k_{fld}, respectively), and the fractional population of the unfolded form in equilibrium (θ_{eq}) were determined.

Structure Analysis. The water ASAs of the Lpp-56 protein, separated helical chains, and peptides in the extended conformation were determined by NACCESS (http://wolf.umist.ac.uk./naccess/). For the molecular graphics, Mole was used.

RESULTS

Melting Profiles of Lpp-56 at Neutral pH. Figure 2A shows the temperature dependencies of the ellipticity of Lpp-56 (inset) and its temperature derivative upon consecutive heatings of the same sample after its slow cooling to the starting temperature of 0 °C at pH 7.4 in the presence 100 mM KCl. It appears that Lpp-56 is fully helical below 50 °C and completely loses its helical conformation over a narrow temperature range of 55−70 °C. This process of unfolding and dissociation of the trimeric coiled coil proceeds with intensive heat absorption, which results in a noticeable heat capacity increment, ΔC_p (Figure 2B). We can consider this process a "melting" of the coiled coil and, correspondingly, denote the temperature of maximum heat absorption as a melting temperature ($T_m = T_{max}$).

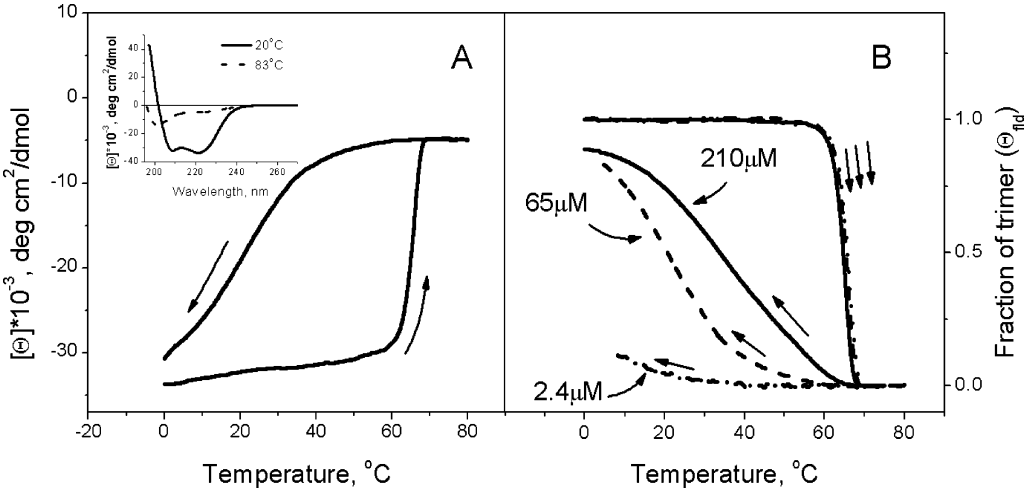

FIGURE 3: (A) Ellipticity profiles of Lpp-56 obtained upon heating and cooling at 65 μM monomers in solution at pH 7.4. The inset shows the ellipticity spectrum of Lpp-56 at 20 and 83 °C. (B) Fraction of the trimers in heating and cooling experiments at different protein concentrations.

The change in ellipticity and the heat absorption peak are largely reproducible on consecutive heating runs of the same sample. The small decrease in the initial ellipticity and of the area of the heat absorption peak on repeated runs results from some degradation of the polypeptide, which typically takes place at high temperatures. The sharpness of the heat absorption peak and its correspondence with the observed changes in ellipticity suggest that the process of unfolding of the Lpp-56 is highly cooperative.

It is notable that the partial heat capacity of Lpp-56 initially increases linearly with an increase in temperature with a rather small slope ($\partial C_p/\partial T = 0.17 \pm 0.01$ kJ K^{-2} mol^{-1} = 9.3 ± 0.5 mJ K^{-2} g^{-1}). Calculated per gram, the specific slope is slightly greater than that for proteins with rigid structure, such as BPTI [$\partial C_p/\partial T = 6.0 \pm 0.5$ mJ K^{-2} g^{-1} (*29*)], but it is significantly smaller than the heat capacity dependencies on temperature of the two-stranded coiled coils (*7*, *9*, *15*, *30*, *31*). This shows that the initial three-stranded coiled-coil structure of Lpp-56 is quite rigid, and an increase in temperature does not significantly intensify fluctuations of its structure until the critical temperature is reached, where it unfolds cooperatively.

Extrapolating the heat capacities of the folded and unfolded states into the transition zone (Figure 2B), one can determine the heat capacity increment upon protein unfolding, ΔC_p, and, from the heat absorption peak area, the enthalpy of unfolding, ΔH^{cal} (Table 1).

The simplest assumption would be that the process of dissociation and unfolding of the three helical strands of Lpp-56 ($F_3 \leftrightarrow 3U$) is a cooperative third-order reaction. One can determine then the van't Hoff enthalpy of this process from its sharpness at the melting temperature, T_m, i.e., from the height of the heat absorption peak, C_p^{max}, normalized to its area, ΔH^{cal}, assuming that $n = 3$ (*28*):

$$\Delta H^{vH}(T_m) = \frac{(\sqrt{n}+1)^2 R T_m^2 C_p^{max}}{\Delta H^{cal}} = \frac{7.46 R T_m^2 C_p^{max}}{\Delta H^{cal}} \qquad (3)$$

The values obtained for ΔH^{vH} are listed in Table 1. Surprisingly, they are in stark conflict with the calorimetrically measured ΔH^{cal}: the van't Hoff enthalpy is almost twice the calorimetric enthalpy. Moreover, Table 1 shows that the unfolding temperature does not depend on concentration as expected for a multimeric reaction. On the other hand, the melting profiles show a substantial dependence on the heating rate (Figure 2C) and especially on the cooling rate (Figure 2D).

Table 1: Calorimetrically Measured Apparent Thermodynamic Characteristics of the Lpp-56 Trimer and Its Unfolding and Dissociation (melting) at pH 7.4 and 3.0[a]

pH	heating rate	concentration	$(\partial C_p/\partial T)$	ΔC_p	T_m	ΔH^{cal}	ΔH^{vH}
7.0[b]	1.0	69.3	0.17	2.5	65.0	660	1150
	0.5	67.7	0.17	–	64.3	676	1080
	0.25	63.7	0.17	–	63.1	657	1073
	0.125	138.3	–	–	61.5	699	1090
3.0[c]	1.0	360	0.25	2.2	43	350	430
	σ		±0.01	±0.2	±0.1	±20	±50

[a] Heating rate in kelvin per minute. Concentration in micromolar trimer. C_p and ΔC_p in kilojoules per kelvin per mole. T_m (the temperature of heat absorption peak maximum) in degrees Celsius. ΔH^{cal} and ΔH^{vH} are enthalpies measured calorimetrically and determined using the van't Hoff equation, respectively, both in kilojoules per mole. $(\partial C_p/\partial T)$ in kilojoules per square kelvin per mole. [b] In 100 mM NaCl, 10 mM sodium phosphate buffer (pH 7.4). [c] In 100 mM NaCl, 10 mM Gly-HCl buffer (pH 3.0).

It is notable that the heat effects in the cooling experiments depend significantly on the concentration, in contrast to the heating experiment. This becomes especially clear using ellipticity as an index of the reaction process, since the CD spectrometer permits variation of protein concentration over a significantly larger range than the DSC instrument (Figure 3).

The significant differences between the profiles obtained on heating and cooling, i.e., the large hysteresis, demonstrate that, in both cases, we do not have thermodynamic equilibrium. This conclusion is confirmed by studying the kinetics of unfolding and refolding of Lpp-56 at different temperatures using CD spectroscopy.

Kinetic Studies of the Lpp-56 Unfolding and Refolding at Neutral pH. By heating the protein solution rapidly to some fixed temperature above the T_m, or cooling rapidly the preheated protein solution below the T_m, one can easily measure the kinetics of the Lpp-56 unfolding and refolding because both processes are slow, proceeding over many minutes and even hours.

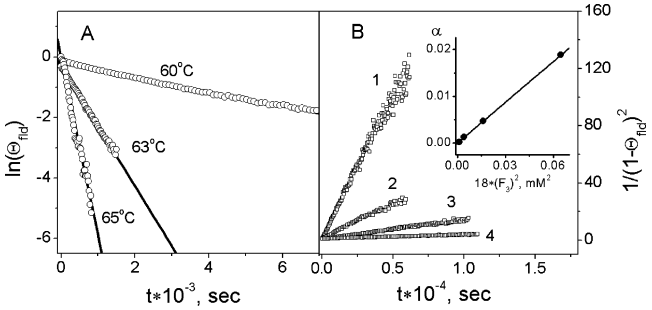

FIGURE 4: (A) Dependence of the logarithm of the fraction of folded Lpp-56 molecules on time, determined in unfolding kinetic experiments using a temperature jump from 20 °C to 60, 63, and 65 °C and 65 μM protein in a pH 7.4 solution. (B) Dependence of the inverse square of the fraction of unfolded Lpp-56 molecules on time, determined in refolding kinetic experiments using a temperature jump from 72 to 25 °C at protein concentrations of 162 (1), 81 (2), 40.6 (3), and 20.3 μM (4). The inset shows the dependence of the slopes, α, of the kinetic functions on protein concentration.

The transition of the folded trimeric coiled coil into unfolded monomers ($F_3 \rightarrow 3U$) is described by the first-order kinetic reaction:

$$\frac{\partial[F_3]}{\partial t} = -k_{unf}[F_3] \quad (4)$$

where k_{unf} is an unfolding rate constant and $[F_3]$ is the concentration of the folded trimer. Its integration gives for the fraction of folded trimers $\theta = [F_3]/[F_3]_0 = \exp(k_{unf}t)$ or

$$\ln(\theta) = -k_{unf}t \quad (5)$$

Figure 4A shows that the logarithm of the fraction of folded molecules, $\ln(\theta)$, is a linear function of time; i.e., this process is indeed a first-order reaction. In contrast, folding of trimer from the unfolded monomers ($3U \rightarrow F_3$) is described by the third-order kinetic reaction

$$\frac{d[U]}{dt} = -k_{fld}[U]^3 \quad (6)$$

The integration of which gives

$$1/(1-\theta)^2 = 1 + 18k_{fld}[F_3]_0^2 t \quad (7)$$

Correspondingly, the kinetic data of the refolding reaction appear as a linear function of time only with respect to $1/(1-\theta)^2$, i.e., in the coordinates linearizing the third-order reaction (Figure 4B). As follows from eq 7, the slope of the kinetic functions ($\alpha = 18k_{fld}[F_3]^2$) for the third-order reaction should be proportional to the square of the concentration of the protein (inset of Figure 4B). The slope defines the rate constant at the given temperature. The rate constants determined by kinetic experiments at various temperatures are listed in Table 2 and in Figure 5 are plotted in Arrhenius coordinates.

According to the Arrhenius equation

$$k = \gamma \exp(-\Delta E^*/RT) \quad (8)$$

the slope of ln k versus $1/RT$ corresponds to the activation energy ΔE^* for the unfolding and refolding reactions. It is notable that the function for the unfolding reaction appears to be linear, which means that the activation energy does not depend noticeably on temperature; i.e., the activation heat capacity effect is close to zero. In contrast, the function for refolding shows substantial curvature, which suggests that the activation energy for refolding depends on temperature. The activation heat capacity of refolding, ΔC_p^*, obtained by fitting the data shown in Figure 5, is equal to -2.4 ± 0.3 kJ K^{-1} mol^{-1}. The activation heat capacity effect thus is very close to the calorimetrically measured total heat capacity increment of Lpp-56 unfolding (Table 1). The fact that the activation heat capacity changes mainly with the transition from the unfolded to the activated state is in agreement with data obtained for many other globular proteins (see ref *32*). The activation energy, ΔE^*, can in fact be considered the activation enthalpy, ΔH^*, since they differ by RT ($\cong$2.7 kJ/mol), i.e., a value which is on the order of our experimental error.

Using transition rate theory, from the observed rate constant one can also determine the activation Gibbs energy, ΔG^*, and the activation entropy, ΔS^*, bearing in mind that the observed rate constant exponentially depends on these two parameters:

$$k = \gamma \exp(-\Delta G^*/RT) = \gamma \exp(-\Delta H^*/RT) \exp(\Delta S^*/R) \quad (9)$$

Table 2: Rate Constants of Lpp-56 Unfolding and Refolding Determined by the CD-Kinetic Experiments at pH 7.4[a]

unfolding[b]		refolding[c]	
T (°C)	k_{unf} (s^{-1})	T (°C)	k_{fld} (M^{-2} s^{-1})
60.0	3.4×10^{-4}	5.0	2.3×10^{6}
63.0	1.9×10^{-3}	15.0	9.2×10^{5}
65.0	6.3×10^{-3}	25.0	2.9×10^{5}
70.0	1.2×10^{-1}	35.0	8.2×10^{4}
–	–	45.0	1.8×10^{4}

[a] The concentration of Lpp-56 in kinetic experiments was 65 μM. [b] For unfolding, the heating jump from 20 °C to 60, 63, 65, and 70 °C was used. [c] For refolding, the cooling jump from 72 °C to 50, 45, 36, 25 15, and 5 °C was used.

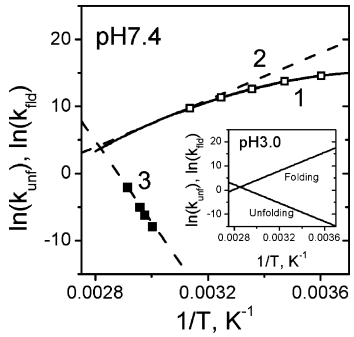

FIGURE 5: Dependence of the logarithm of the rate constants of unfolding (■) and refolding (□) of Lpp-56 at pH 7.4 on the inverse temperature as determined from the CD-kinetic experiments. For unfolding, rapid heating from 20 °C to 60, 63, 65, and 70 °C was used; for refolding, rapid cooling from 72 °C to 45, 36, 25, 15, and 5 °C was used. The dependence is linear for unfolding and shows clear curvature for refolding [the fitted function is shown as the solid line (1)]. It means that unfolding proceeds with an activation heat capacity effect close to zero, but refolding is associated with a significant negative activation heat capacity change. The dashed lines (2 and 3) show the functions determined by fitting the DSC-melting profiles of Lpp-56. The inset shows the functions of the logarithm of the rate constants of unfolding and refolding of Lpp-56 obtained by fitting the DSC-melting profiles at pH 3.0.

Table 3: Activation Parameters of Lpp-56 Unfolding and Refolding at pH 7.4 and 3.0 at Their Equilibrium Temperatures, T_t^{eq} [a]

	unfolding				folding			
conditions	ΔH^*	ΔG^*	$T\Delta S^*$	ΔC_p^*	ΔH^*	ΔG^*	$T\Delta S^*$	ΔC_p^*
pH 7.4, $T_t^{eq} = 60$ °C	501	105[c]	396[cc]	0	−140	57[cc]	−190[cc]	−2.4
		84[cd]	417[cd]			35[cd]	−175[cd]	
pH 3.0, $T_t^{eq} = 40$ °C	158	93[cc]	66[cc]	0[cb]	−160	59[cc]	−220[cc]	0[cb]
		75[cd]	83[cd]			41[cd]	−201[cd]	
σ	±30	±8	±15	±0.3	±10	±5	±15	±0.3

[a] ΔH^*, ΔG^*, and $T\Delta S^*$ are in kilojoules per mole. ΔC_p^* is in kilojoules per kelvin per mole. [b] ΔC_p^* taken equal to zero at global fitting of the kinetic data. [c] Values calculated by Eyring's formalism. [d] Values calculated by Kramers' formalism.

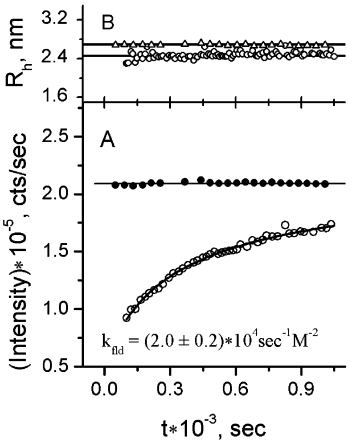

FIGURE 6: (A) Time dependence of the light scattering intensity in the refolding experiment after a fast drop in temperature of an Lpp-56 solution from 72 to 50 °C (○). The protein concentration in solution was 2.0 mg/mL. The solid line is the best fit of the experimental data by the function corresponding to a third-order reaction. The filled circles show that the intensity of light scattering by folded Lpp-56 at 4 °C does not change over time. (B) Hydrodynamic radius determined from the light scattering experiment for the native protein at 4 °C (△) and for the refolding process at 50 °C (○).

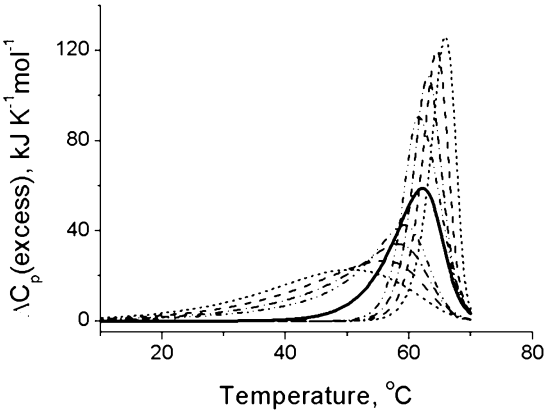

FIGURE 7: Simulated melting profiles of Lpp-56 for the heating and cooling rates of 1.0, 0.5, 0.25, and 0.125 K/min (dashed lines) and the equilibrium melting profile (thick line). For simulation, the thermodynamic parameters obtained at pH 7.4 were used (Tables 2 and 3).

However, in contrast to ΔH^*, the value of which does not depend on the preexponential coefficient (see eq 4), the values of ΔG^* and ΔS^* depend on the preexponential coefficient γ, the value of which is not precisely determined and, depending on the formalism that is chosen, varies over the range from 6.2×10^{12} M^{-1} s^{-1} according to Eyring's formalism (*33*) to 3.3×10^9 M^{-1} s^{-1} according to Kramers' formalism (*34*) (see also refs *9*, *32*, and *35*). This leads to some uncertainty in the values of ΔG^* and ΔS^*, as shown in Table 3, which in the case of the entropy is relatively small but is significant in the case of the Gibbs energy.

Dynamic Light Scattering Experiment. Similar refolding experiments were also carried out using the dynamic light scattering method. Figure 6 shows that the intensity of light scattering by the Lpp-56 solution, which was preheated to 72 °C and cooled rapidly to 50 °C, increases with time and tends to the value which it had initially at 4 °C before being heated. One can see that the experimental points are perfectly approximated by the function describing a one-stage third-order kinetic process with the folding rate constant at 50 °C equaling $(2.0 \pm 0.2) \times 10^4$ M^{-2} s^{-1}. This rate constant corresponds well with the rate constant determined by CD-kinetic experiments at that temperature (Table 2). It is notable that, notwithstanding a significant change in intensity of the light scattering in the cooled solution, the hydrodynamic radius of the particles, which are responsible for scattering, does not change and is close to the hydrodynamic radius of the molecules before they were heated above the melting point of Lpp-56. This means that the observed increase in light scattering intensity results from the increase in the concentration of the particles responsible for the light scattering, the folded trimers, and the monomers do not contribute noticeably to this effect. This is surprising because one might expect that refolding of the helical trimer from the unfolded monomers proceeds through a dimeric helical intermediate. However, the light scattering method does not detect the appearance of intermediate dimers. The situation with Lpp-56 thus differs qualitatively from that of LZ16A, the only studied three-stranded coiled coil, which showed the presence of dimeric intermediates in the folding reaction (*17*).

Simulation of the Heating−Cooling Excess Heat Capacity Profiles of Lpp-56. Because of the slow unfolding−refolding reactions, the heat capacity profiles of Lpp-56 depend significantly on the scanning rate, in contrast to the profiles of other coiled coils (*7*). Using the rate constants and the activation energies obtained in the kinetic experiments, one can simulate the excess heat capacity profiles of Lpp-56 unfolding and refolding for the various heating and cooling rates (see Materials and Methods).

The simulated profiles of Lpp-56 unfolding and refolding, shown in Figure 7, illustrate the experimentally observed evolution of the apparent excess heat capacity functions obtained at different heating and cooling rates (Figure 2). One can see that with an increase in the heating rate, the heat absorption peak shifts to temperatures higher than that corresponding to the equilibrium process and its high-

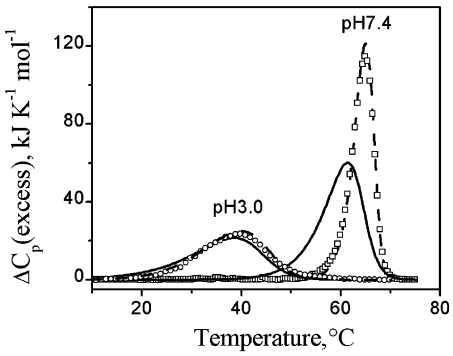

FIGURE 8: Equilibrium excess heat capacity functions of Lpp-56 at pH 7.4 and 3.0 (solid lines) determined by fitting of the apparent excess heat capacity profiles (○ and □) obtained calorimetrically upon heating with a rate of 1 K/min at a protein concentration of 3×10^{-5} M. The dashed line shows the fitted apparent excess heat capacity function.

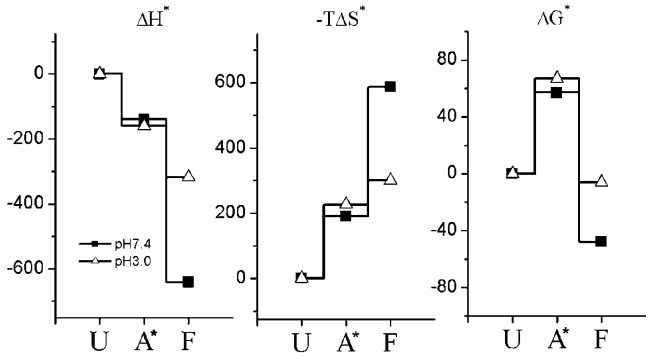

FIGURE 9: Scheme of the energy levels of Lpp-56 corresponding to the native folded (F), unfolded (U), and activated (A*) states at 60 °C and pH 7.4 (■) and pH 3.0 (△) in the presence of 100 mM KCl and at a protein concentration of 3×10^{-5} M. ΔH^* is the activation enthalpy, $T\Delta S^*$ the activation entropy factor, and ΔG^* the activation Gibbs free energy, all in kilojoules per mole. To not overload the figure, the activation energies calculated only by Eyring's formalism are shown.

temperature slope becomes steeper, while the low-temperature slope becomes shallower. An increase in the cooling rate results in the opposite effect.

Fitting of the DSC-Melting Profiles. Using eq 2 and the 3M-kinetics program, one can also solve the reverse problem, which is to calculate the equilibrium excess heat capacity function and kinetic parameters from the apparent nonequilibrium functions obtained at different heating and cooling rates. It appears that at the concentration of the Lpp-56 trimer ($[F_3]_0 = 3 \times 10^{-5}$ M), the equilibrium transition temperature, T_t, is 60 °C at pH 7.4, but at pH 3.0, it drops to 40 °C. The solid lines in Figure 8 show the calculated equilibrium excess heat capacity functions. The fitting of these profiles, assuming for simplicity that the activation heat capacities for folding and unfolding reactions are zero, gives us the rate constants of these reactions in the whole considered temperature range. The dashed lines in Figure 5 show these functions for pH 7.4 and 3.0. One can see that, for the unfolding reaction at pH 7.4, the derived function of the rate constant is in excellent agreement with the experimentally determined values given as black squares.

For the folding reaction at this pH, the derived function of the rate constant is in agreement with the experimental points (white squares) at temperatures close to the equilibrium transition temperature, but at significantly lower temperatures, they deviate because the derived function was obtained with the assumption that activation enthalpy does not change with temperature. The rate constants of Lpp-56 unfolding and refolding at pH 3.0 were obtained with the same assumption, $\Delta C_p^* = 0$ (inset of Figure 5). The decrease in pH has changed considerably the rate constants, especially that of the unfolding reaction. It is notable, however, that the functions of the rate constants for the unfolded and folded reaction at both considered pHs cross each other when $1/T = 0.00283$ K^{-1}, i.e., at $T \sim 80$ °C. This is a temperature, T_G, where the Gibbs energy difference between the folded and unfolded states is zero at the standard protein concentration, 1 M.

DISCUSSION

Energy Barriers. The most remarkable feature of the unfolding and refolding of Lpp-56 is that the rate is unusually slow, particularly at pH 7.4. It is much slower than that of any two-stranded coiled coils that have been studied (*30*). Moreover, it is several orders of magnitude slower than the unfolding and refolding of LZ16A, the only three-stranded coiled coil that has been studied (*17*). This coiled coil, however, demonstrated the presence of dimeric intermediates in the folding reaction in contrast to Lpp-56, which, as we have shown, refolds without detectable dimeric intermediates. The absence of dimeric intermediates in the refolding of Lpp-56 may explain its very slow rate: the probability of proper alignment of all three strands is rather low, but as soon as it is achieved, all three strands cooperatively collapse into a thee-stranded coiled coil.

The slow unfolding and refolding rates of Lpp-56 indicate that the activation barriers in these reactions are unusually high (Figure 9). It appears that at pH 7.4 the major changes in enthalpy and entropy take place with the transition from the folded to the activated state. The activation enthalpy at this stage definitely dominates over the activation entropy factor. Their difference forms a Gibbs free energy barrier of ~100 kJ/mol when the trimeric coiled coil reaches the unfolded and dissociated state. The transition from the unfolded state to the activated state is much easier and is associated with significantly smaller changes in enthalpy and entropy, but it is notable that the entropy factor dominates at this stage. The overall change in the enthalpy of Lpp-56 upon the transition from the folded to the unfolded state (i.e., the difference between the activation enthalpies for the two stages) amounts to 640 kJ/mol at pH 7.4. This value perfectly corresponds with the calorimetrically determined enthalpies of Lpp-56 unfolding under these conditions (Table 1).

According to the Arrhenius plot presented in Figure 5, the activation heat capacity does not change noticeably with the transition from the folded to the activated state, but it clearly increases by ~2.4 kJ K^{-1} mol^{-1} with the transition from the activated state to the unfolded state. The value of this activation heat capacity effect amounts to the calorimetrically measured heat capacity increment of Lpp-56 unfolding (Table 1).

It is known that the heat capacity effect of conformational changes in proteins is mostly caused by hydration of exposed apolar groups (*29*). This suggests that the transition of Lpp-56 from the native state to the transition one does not result in the hydration of apolar groups. It thus appears that the

apolar groups, which are packed in the interior of the trimeric coiled coil, are still inaccessible to water in the activated state. That is, the helices forming this coiled coil are still not sufficiently separated to permit water penetration. In contrast, the change from the transition state to the unfolded state is likely to be associated with the extensive hydration of apolar groups. On the other hand, the transition of folded Lpp-56 into the transition state is associated with a significant increase in enthalpy and entropy. It thus appears that, at this stage, extensive disruption of some short-range enthalpic interactions takes place, resulting in a considerable increase in the degree of conformational freedom of interfacial groups. These cannot be hydrogen bonds, especially between those residues, which form the interface in the coiled coil and are removed from water because their disruption without hydration requires too much energy. In this stage, therefore, disruption of interhelical van der Waals contacts most probably takes place. The overall contact area of apolar groups in the interface of the Lpp-56 coiled coil, determined by rolling a probe over the surface of the coiled coil and the isolated helices, is $\sim 4.4 \times 10^3$ Å^2/mol. The averaged surface-normalized energy of van der Waals interactions in proteins is on the order of 120 J/Å^2 (*29*). One can expect therefore that the energy of disruption of van der Waals contacts in Lpp-56 should be ~530 kJ/mol. This value is surprisingly close to the observed activation energy upon unfolding of the trimeric coiled coil, 500 kJ/mol (Table 3). Disruption of the interfacial van der Waals contacts should unfreeze the side chains of residues, which are packed in the interface. Analysis of the Lpp-56 structure shows that there are ~72 side chains that gain freedom when the interhelical contacts are disrupted. If we assume that the entropy of unfreezing of the mean side chain is ~13 J K^{-1} mol^{-1} (*36*), for 72 residues this gives an entropy gain of ~1.0 kJ K^{-1} mol^{-1}, a value within the limits for the derived activation entropy at this stage [1.2 ± 0.2 kJ K^{-1} mol^{-1} (Table 3)].

It appears thus that unfolding of the rigid three-stranded coiled coil starts from the simultaneous disruption of all van der Waals contacts between the strands, and since the probability of that is low, the process is slow.

According to the considered model, during the transition from the activated state to the unfolded state, water penetrates between the separated helices hydrating the exposed apolar groups and, by decreasing the strength of intrahelical hydrogen bonds at the apolar face, initiates unfolding of the helices. The hydrated surface area of the exposed apolar groups (8.8×10^3 Å^2/mol) is twice that of the area of apolar contacts. The surface-normalized enthalpy of hydration of apolar groups at 50 °C is approximately −70 J/Å^2 (*29*). Thus, the overall enthalpy of hydration of exposed apolar groups is expected to be approximately −600 kJ/mol. On the other hand, the enthalpy of disruption of an isolated α-helix at 60 °C amounts to 4.5 kJ per residue (*7*). For the 168 residues, which form three helices of Lpp-56, this gives ~760 ± 20 kJ/mol. The net sum of these two values, which are opposite in sign, is ~160 kJ/mol, and this is close to the enthalpy of the transition from the activated state to the unfolded state (Table 3). The entropy for the transition from the activated state to the unfolded state can be calculated bearing in mind that the entropy of unfolding of an α-helix at 60 °C is ~ 20 J K^{-1} (mol per residue)$^{-1}$ (*7*), the entropy of hydration of the aliphatic groups (ΔS^{hyd}) equals −0.57 J K^{-1} mol^{-1} Å^{-2} (*29*), and the ASA of the apolar groups, which are hydrated upon dissociation of strands, is ~4400 Å^{-2} mol^{-1}. This makes the activation entropy factor ($-T\Delta S^*$) 250 kJ/mol, which is very close to that determined by studying the refolding kinetics (Figure 7).

In the folding reaction, according to the model that follows from the kinetic studies, the transition into the activated state consists of folding the separate strands into a helical conformation and the proper alignment of the three helices at a distance, which excludes water, but is insufficient to form van der Waals contacts. The probability of folding into an α-helical conformation for the isolated strands of Lpp-56 is very low; at a low protein concentration, we do not observe the appearance of helical conformation by CD, even at low temperatures (see Figure 3). The low folding propensity of the Lpp-56 strands is perhaps caused by the presence of charged residues (Figure 1), which give rise to considerable repulsive forces destabilizing the helical conformation of the strands. However, the same forces would align the folded helices in parallel and in register so that the apolar sides face each other and the oppositely charged groups may form salt links, which are important for the formation of the trimeric coiled coil (see below) (*23*).

A decrease in pH significantly decreases the enthalpy and entropy for the transition from the folded to the activated state.

Lpp-56 in an Acidic Solution. Unfolding of Lpp-56 at pH 3.0 was studied especially to investigate the role of salt links in the formation of this trimeric coiled coil. Under these conditions, the Asp residues are protonated, and that eliminates the salt links between these residues and Lys. As shown above, this results in the significant destabilization of Lpp-56; at pH 3.0, it unfolds upon heating at a much lower temperature and with a much lower enthalpy than at pH 7.4 (Table 1 and Figure 8). Analysis of the observed unfolding−refolding profiles using the above-described formalism showed that a decrease in pH resulted in a significant drop in the enthalpy and entropy for the transition from the folded to the activated state (Table 3 and Figure 9).

A considerable decrease in the unfolding enthalpy at pH 3.0 is surprising because the salt links were assumed to be entropic interactions, and in themselves, they cannot contribute much to the enthalpy of protein stabilization. It appears, however, that they play an essential role in the formation of the three-stranded coiled-coil structure of Lpp-56. Namely, they might be important for aligning the strands in proper register, which is required for formation of the tight van der Waals contacts between the apolar groups of the strands. The folded state of Lpp-56 at pH 3.0, therefore, is looser than at pH 7.4. Correspondingly, the enthalpy and entropy for the transition from the folded to the activated state are smaller. The assumption that the structure of Lpp-56 at pH 3.0 is looser than at pH 7.4 is confirmed by the steeper initial slope of the heat capacity of Lpp-56, showing that heating at pH 3.0 proceeds with a more significant increase in thermal fluctuations of its structure (Table 1). Actually, a similar situation was observed upon replacement of some key residues in Lpp-56; this resulted in looser packing of the triple-helical coiled coil and a significant increase in its *B*-factor (*23*).

Thermodynamic Characteristics of Lpp-56 Unfolding. The equilibrium transition temperature, T_t, which is derived from

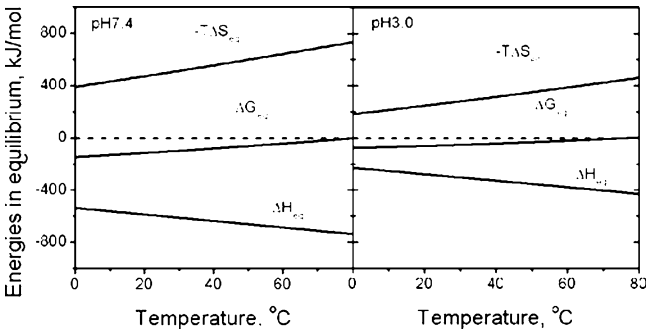

FIGURE 10: Thermodynamic functions of the equilibrium unfolding and refolding of Lpp-56 at pH 7.4 and 3.0.

the apparent heat capacity profiles, permits us to determine the equilibrium unfolding enthalpy at this temperature using the calorimetrically measured heat capacity increment, ΔC_p:

$$\Delta H_t = \Delta H_m - \Delta C_p(T_m - T_t) = 640 \text{ kJ/mol} \quad (10)$$

The equilibrium Gibbs energy of unfolding at T_t and the concentration of the protein ($[F_3]_0$) according to the equation for the dissociation of the homotrimer (*28*) equal:

$$\Delta G_t = -RT_t \ln([F_3]_0^2 \times 0.5^2 \times 3^3) = 55 \text{ kJ/mol} \quad (11)$$

This equilibrium Gibbs energy is very close to the difference in the activation Gibbs energies for the folding and unfolding reactions (Figure 7 and Table 3). The equilibrium entropy of unfolding under this condition is

$$\Delta S_t = (\Delta H_t - \Delta G_t)/T_t = 1.77 \text{ kJ K}^{-1} \text{ mol}^{-1} \quad (12)$$

At any other temperature, T, the thermodynamic parameters of cooperative unfolding of Lpp-56 can be determined by simple extrapolations:

$$\Delta H(T) = \Delta H(T_t) - \Delta C_p(T_t - T) \quad (13)$$

$$\Delta S(T) = \Delta S(T_t) - \Delta C_p \ln(T_t/T) \quad (14)$$

$$\Delta G(T) = \Delta H(T) - T\Delta S(T) \quad (15)$$

These functions for Lpp-56 at pH 7.4 and 3.0 in the presence of 100 mM KCl are shown in Figure 10.

It appears that the Gibbs energy of Lpp-56 stabilization at 4 °C equals −137 kJ/mol. This value is significantly higher than −85 kJ/mol, the Gibbs energy of Lpp-56 stabilization at this temperature found from its guanidinium chloride-induced denaturation treated as an equilibrium reaction (*23*). At that time, however, it was not realized yet that the observed changes in Lpp-56 do not represent an equilibrium reaction. This figure also shows that the temperature at which ΔG_{eq} becomes zero, T_G, is 80 °C, just as found from the crossing of the rates of the unfolding and refolding reactions (Figure 5). The large difference between the T_G and the equilibrium transition temperature, T_t (i.e., the temperature at which half of molecules are in the unfolded state at equilibrium), results from the fact that ΔG is zero at T_t for only first-order reactions.

The enthalpy and entropy of Lpp-56 cooperative unfolding at pH 3.0 are significantly lower than the enthalpy and entropy, respectively, of the cooperative unfolding at pH 7.4, if compared at the same temperature. This shows that their structures are not identical. As discussed above, the structure of Lpp-56 at pH 3.0 is much looser. Therefore, we can expect that at 20 °C, the contribution of the enthalpy of van der Waals interactions between the apolar groups to protein folding energetics is not balanced by the enthalpy of dehydration of these groups; i.e., the enthalpy of hydrophobic interactions is not zero at this temperature as it is in the case of the proteins with tightly packed interiors (*29*). In contrast, we can expect that at pH 7.4 the enthalpy of the hydrophobic contribution to the stabilization of the Lpp-56 structure is zero at 20 °C. Under these conditions, the full enthalpy of unfolding of this protein at this temperature should correspond to the contribution of hydrogen bonds in its stabilization.

The enthalpy of Lpp-56 unfolding extrapolated to 20 °C is ΔH(20 °C) (536 ± 40 kJ/mol). Assuming that it results from the disruption of 186 hydrogen bonds, the enthalpy of hydrogen bonds in Lpp-56 appears to be 2.9 ± 0.2 kJ/mol. This value is very close to the previously determined enthalpy of hydrogen bonding in the individual α-helix (*13*) and the double-stranded coiled coils (*7*).

CONCLUSION

Characterization of protein stability by their melting profiles obtained either optically or by DSC is now widely used. An important conclusion, which follows from the above, is that by the apparent sharp and reproducible melting profile of protein, one cannot judge if a protein's unfolding represents an equilibrium cooperative transition and estimate from its shape the thermodynamic characteristics of protein stability. To specify the temperature-induced process thermodynamically, one should be sure that the observed process is reversible and represents equilibrium. This requires its investigation in both the heating and cooling experiments carried out at different rates. The same requirement holds for the denaturant-induced unfolding of proteins: to be sure that the observed isotherm does indeed reflect equilibrium, one has to obtain it at increasing and decreasing denaturant concentrations.

If the observed melting profiles of protein do not correspond to equilibrium, which is very frequently the case with proteins, one can determine the equilibrium parameters of protein unfolding using the above-described formalism. Moreover, this formalism permits one to determine not only the equilibrium thermodynamic parameters but also the rate constants of the unfolding−refolding reactions over a broad temperature range and, correspondingly, the activation parameters specifying the energy barrier between the folded and unfolded states.

Applying the developed method of analysis of the melting profiles to Lpp-56, we showed that formation of this three-stranded coiled coil is a very slow process because it requires proper alignment of all three strands in a helical conformation. As soon as it is achieved, however, all three strands cooperatively collapse into a three-stranded coiled coil. Unfolding of this rigid structure proceeds even slower, since that requires simultaneous breaking of all van der Waals contacts and salt links between the strands, and this presents a large energy barrier and takes a long time.

ACKNOWLEDGMENT

We thank Neville Kallenbach for stimulating us to do this work and Victoria Hargreaves for critical reading of the manuscript.

SUPPORTING INFORMATION AVAILABLE

Kinetic analysis of the apparent excess heat capacity profiles. This material is available free of charge via the Internet at http://pubs.acs.org.

REFERENCES

1. Baldwin, R. L., and Rose, G. D. (1999) Is protein folding hierarchic? II. Folding intermediates and transition states, *Trends Biochem. Sci. 24*, 77−83.
2. Baldwin, R. L., and Rose, G. D. (1999) Is protein folding hierarchic? I. Local structure and peptide folding, *Trends Biochem. Sci. 24*, 26−33.
3. Kim, P. S., and Baldwin, R. L. (1990) Intermediates in the folding reactions of small proteins, *Annu. Rev. Biochem. 59*, 631−660.
4. Myers, J. K., and Oas, T. G. (1999) Reinterpretation of GCN4-p1 folding kinetics: partial helix formation precedes dimerization in coiled coil folding, *J. Mol. Biol. 289*, 205−209.
5. Baldwin, R. L. (1995) α-Helix formation by peptides of defined sequence, *Biophys. Chem. 55*, 127−135.
6. Bosshard, H. R., Durr, E., Hitz, T., and Jelesarov, I. (2001) Energetics of coiled coil folding: the nature of the transition states, *Biochemistry 40*, 3544−3552.
7. Dragan, A. I., and Privalov, P. L. (2002) Unfolding of a leucine zipper is not a simple two-state transition, *J. Mol. Biol. 321*, 891−908.
8. Hodges, R. S., Semchuk, P. D., Taneja, A. K., Kay, C. M., Parker, J. M., and Mant, C. T. (1988) Protein design using model synthetic peptides, *Pept. Res. 1*, 19−30.
9. Ibarra-Molero, B., Makhatadze, G. I., and Matthews, C. R. (2001) Mapping the energy surface for the folding reaction of the coiled-coil peptide GCN4-p1, *Biochemistry 40*, 719−731.
10. Kohn, W. D., Kay, C. M., and Hodges, R. S. (1998) Orientation, positional, additivity, and oligomerization-state effects of interhelical ion pairs in α-helical coiled-coils, *J. Mol. Biol. 283*, 993−1012.
11. Scholtz, J. M., Marqusee, S., Baldwin, R. L., York, E. J., Stewart, J. M., Santoro, M., and Bolen, D. W. (1991) Calorimetric determination of the enthalpy change for the α-helix to coil transition of an alanine peptide in water, *Proc. Natl. Acad. Sci. U.S.A. 88*, 2854−2858.
12. Scholtz, J. M., and Baldwin, R. L. (1992) The mechanism of α-helix formation by peptides, *Annu. Rev. Biophys. Biomol. Struct. 21*, 95−118.
13. Taylor, J. W., Greenfield, N. J., Wu, B., and Privalov, P. L. (1999) A calorimetric study of the folding-unfolding of an α-helix with covalently closed N- and C-terminal loops, *J. Mol. Biol. 291*, 965−976.
14. Thompson, K. S., Vinson, C. R., and Freire, E. (1993) Thermodynamic characterization of the structural stability of the coiled-coil region of the bZIP transcription factor GCN4, *Biochemistry 32*, 5491−5496.
15. Yu, Y., Monera, O. D., Hodges, R. S., and Privalov, P. L. (1996) Ion pairs significantly stabilize coiled-coils in the absence of electrolyte, *J. Mol. Biol. 255*, 367−372.
16. Boice, J. A., Dieckmann, G. R., DeGrado, W. F., and Fairman, R. (1996) Thermodynamic analysis of a designed three-stranded coiled coil, *Biochemistry 35*, 14480−14485.
17. Durr, E., and Bosshard, H. R. (2000) Folding of a three-stranded coiled coil, *Protein Sci. 9*, 1410−1415.
18. Harbury, P. B., Zhang, T., Kim, P. S., and Alber, T. (1993) A switch between two-, three-, and four-stranded coiled coils in GCN4 leucine zipper mutants, *Science 262*, 1401−1407.
19. Harbury, P. B., Kim, P. S., and Alber, T. (1994) Crystal structure of an isoleucine-zipper trimer, *Nature 371*, 80−83.
20. Betz, S. F., Bryson, J. W., and DeGrado, W. F. (1995) Native-like and structurally characterized designed α-helical bundles, *Curr. Opin. Struct. Biol. 5*, 457−463.
21. DeGrado, W. F., Wasserman, Z. R., and Lear, J. D. (1989) Protein design, a minimalist approach, *Science 243*, 622−628.
22. Braun, V. (1975) Covalent lipoprotein from the outer membrane of *Escherichia coli*, *Biochim. Biophys. Acta 415*, 335−377.
23. Liu, J., Cao, W., and Lu, M. (2002) Core side-chain packing and backbone conformation in Lpp-56 coiled-coil mutants, *J. Mol. Biol. 318*, 877−888.
24. Shu, W., Liu, J., Ji, H., and Lu, M. (2000) Core structure of the outer membrane lipoprotein from *Escherichia coli* at 1.9 Å resolution, *J. Mol. Biol. 299*, 1101−1112.
25. Liu, Y., and Sturtevant, J. M. (1995) Significant discrepancies between van't Hoff and calorimetric enthalpies. II, *Protein Sci. 4*, 2559−2561.
26. Naghibi, H., Tamura, A., and Sturtevant, J. M. (1995) Significant discrepancies between van't Hoff and calorimetric enthalpies, *Proc. Natl. Acad. Sci. U.S.A. 92*, 5597−5599.
27. Privalov, G. P., and Privalov, P. L. (2000) Problems and prospects in microcalorimetry of biological macromolecules, *Methods Enzymol. 323*, 31−62.
28. Privalov, P. L., and Potekhin, S. A. (1986) Scanning microcalorimetry in studying temperature-induced changes in proteins, *Methods Enzymol. 131*, 4−51.
29. Makhatadze, G. I., and Privalov, P. L. (1995) Energetics of protein structure, *Adv. Protein Chem. 47*, 307−425.
30. Durr, E., Jelesarov, I., and Bosshard, H. R. (1999) Extremely fast folding of a very stable leucine zipper with a strengthened hydrophobic core and lacking electrostatic interactions between helices, *Biochemistry 38*, 870−880.
31. Marti, D. N., Jelesarov, I., and Bosshard, H. R. (2000) Interhelical ion pairing in coiled coils: solution structure of a heterodimeric leucine zipper and determination of pK_a values of Glu side chains, *Biochemistry 39*, 12804−12818.
32. Bilsel, O., and Matthews, C. R. (2000) Barriers in protein folding reactions, *Adv. Protein Chem. 53*, 153−207.
33. Glasstone, S., Laidler, K. J., and Eyring, H. (1940) *Theory of rate processes*, McGraw-Hill, New York.
34. Kramers, H. A. (1940) Brownian motion in a field of force and the diffusional model of chemical reactions, *Physica 7*, 284−304.
35. Gloss, L. M., and Matthews, C. R. (1998) The barriers in the bimolecular and unimolecular folding reactions of the dimeric core domain of *Escherichia coli* Trp repressor are dominated by enthalpic contributions, *Biochemistry 37*, 16000−16010.
36. Pickett, S. D., and Sternberg, M. J. (1993) Empirical scale of side-chain conformational entropy in protein folding, *J. Mol. Biol. 231*, 825−839.

BI048365+